ADVANCED FUNCTIONAL MATERIALS
www.afm-journal.de

Materials Views
www.MaterialsViews.com

FULL PAPER

Nanogel-Incorporated Physical and Chemical Hybrid Gels for Highly Effective Chemo–Protein Combination Therapy

Xilong Wu, Chaoliang He, Yundi Wu, Xuesi Chen, and Jianjun Cheng**

Chemo- and protein-based therapeutics are two major modalities for the treatment of malignant tumors with drastically different therapeutic indices, toxicity, and other pharmacological properties. For intended in vivo applications, they also have distinctly different formulation challenges to be addressed separately. In this study, we attempt to overcome the formulation barriers of chemo- and protein-based therapeutics, and report the development of injectable nanogels, a class of crosslinked physical and chemical composite gels (nPCGs), for the joint delivery of doxorubicin (DOX), protein cytokines recombinant human interleukin-2 (IL-2), and recombinant human interferon-gamma (IFN-γ). The nPCGs are designed through a quick gelation induced by ionic crosslinking of 4-arm poly(ethylene glycol)-*b*-poly(L-glutamic acid) (PPLG) and hydroxypropyl chitosan/4-arm poly(ethylene glycol)-*b*-poly(L-lysine) (HPCS/PPLL), followed by the formation of covalent bonds via a Schiff-base reaction of the oxidized, cholesterol-bearing dextran (OCDEX) nanogels with HPCS/PPLL, which results in increased hydrogel moduli (*G'* around 13.8 kPa) and improved stability. This nPCG, which contains DOX, IL-2, and IFN-γ, shows a synergistic anticancer efficacy through the regulation of apoptosis-related genes in Janus kinase/signal transducer and activator of transcription (JAK/STAT) pathways and mitochondrial pathways in xenograft tumor-bearing mice.

1. Introduction

Most protein drugs tend to lose their biological activity because their delicate conformation and unstable structures are not up against enzymatic degradation and recognition by the host immune systems.[1] The severe side effects induced by high-dose chemotherapy, such as cardiotoxicity and peripheral neurotoxicity,[2] limit its therapeutic efficacy. Thus, the development of drug-delivery systems capable of protecting the active agents from proteolytic and chemical degradation and decreasing drug-related toxicity is of great importance. Although the development of monotherapies based on either small molecules or protein drugs using various delivery technologies is certainly a very active area of research for cancer treatment, combination therapy has shown an even larger potential as an alternative to monotherapy by targeting different apoptosis pathways simultaneously, leading to synergistic anticancer effects.[3,4] Typical combination therapies involve the co-delivery of two chemotherapeutic agents[5,6] or the combination of chemotherapy with another type of therapy, such as immunotherapy,[7,8] hormone therapy,[9] radiation therapy,[10] or gene therapy.[11] There has been great interest in using protein therapeutics, such as monoclonal antibodies,[12] cytokines,[13,14] and enzymes,[15] to enhance the cytotoxicity of chemotherapeutic agents. For instance, it has been reported that the co-administration of selumetinib (a mitogen-activated protein kinase MAPKK inhibitor) and docetaxel (a chemotherapeutic agent) was more efficacious than docetaxel monotherapy in treating Kras and Kras/p53 lung cancers.[7] Another co-delivery strategy utilizing bevacizumab plus fluoropyrimidine-cisplatin also remarkably increased progression-free survival, as well as the overall response rate in the first-line treatment of advanced gastric cancer.[16] But to our knowledge, the exact mechanism of synergistic antitumor activity through a co-delivery system integrating protein drugs and chemotherapeutic agents still remains abstruse.

Herein, we designed a long-acting formulation of nanogel-integrated, physical and chemical composite gels (nPCGs) for co-delivery of recombinant human interleukin-2 (IL-2), recombinant human interferon-gamma (IFN-γ), and doxorubicin (DOX). The resultant gels were subcutaneously implanted into the tumor regions of athymic mice (BALB/c-nu) for the unprecedented combination antitumor therapy based on three agents. DOX, a first-line chemotherapeutic agent, has a broad spectrum of activity against a variety of cancers,[17] such as melanoma, lung, breast, and prostate cancer; it kills cancer cells by intercalating with the nucleobase of DNA, which induces cell apoptosis.[18] But its clinical use often results in undesired cardiotoxicity.[19] IL-2 and Type II interferon (IFN-γ) are activated T-helper (T_h) cells-derived cytokines, which play a key role in

X. L. Wu, Dr. C. L. He, Y. D. Wu, Prof. X. S. Chen
Key Laboratory of Polymer Ecomaterials
Changchun Institute of Applied Chemistry
Chinese Academy of Sciences
5625 Renmin Street, Changchun 130022, P. R. China
E-mail: xschen@ciac.ac.cn
X. L. Wu
University of Chinese Academy of Sciences
Beijing 100049, P. R. China
Prof. J. J. Cheng
Department of Materials Science and Engineering
University of Illinois at Urbana-Champaign
MC 246, 1304 West Green Street, Urbana, Illinois 61801, USA
E-mail: jianjunc@illinois.edu

DOI: 10.1002/adfm.201502742

 © 2015 WILEY-VCH Verlag GmbH & Co. KGaA, Weinheim

the activation and proliferation of tumor-infiltrating lymphocytes (TILs).[20,21] IL-2 has been approved by the Food and Drug Administration (FDA) for the treatment of metastatic renal carcinoma and melanoma.[22] Human IL-2 prepared by recombinant DNA technology has also shown encouraging anti-tumor activity.[23] IFN-γ plays a central role in various anti-proliferative, anti-viral, and immunomodulatory treatments[24,25] and has also been used for many years in clinics for the treatment of chronic granulomatous disease.[26] Recombinant IFN-γ expressed in *Escherichia coli* has been deemed a promising antitumor agent to inhibit the growth of breast cancer cells and melanoma cells,[27] and treat hepatocellular carcinoma (HCC) and metastatic renal-cell carcinoma.[26] Our findings suggest that nPCG carriers could retain the long-term effects of the induced JAK/STAT and mitochondrial pathways of all three active anticancer agents, which can regulate tumor cell survival directly through the STAT5, STAT1, and p53 associated anti-/pro-apoptotic cascades, resulting in the apoptosis of tumor cells. Insights from this new combined chemo-protein treatment against cancer may open the way for improved cytokine therapy to treat the disease.

In-situ gelling hydrogels and hydrogels that are injectable have attracted substantial attention as local delivery carriers because of their capacity to minimize the systemic drug concentration and avoid the high risk of surgery.[28–31] These hydrogel formulations can be prepared using various physical or chemical crosslinking methods.[32–34] Nevertheless, the burst release of drugs remains a key drawback for injectable formulations.[35,36] The weak mechanical properties of hydrogels that are formed solely via physical interactions normally result in gels with low structural stabilities, which may lead to an undesired, rapid loss of the therapeutic functions of the drug in vivo.[35,37] Chemically crosslinked hydrogels often have slow gelation kinetics, which may result in the loss of drugs from the gels and distribution to other parts of the body.[36] **Figure 1** shows the schematic illustration of the nanogel-incorporated physical and chemical hybrid gels we have designed, which contain IL-2, IFN-γ, and DOX. Previous studies have shown that nanogel-embedded hydrogel composites could improve the kinetic release profile of the drug by affording a nanoscale reservoir barrier, which reduced or even removed the burst-release effects of drugs in hydrogel or nanogel drug-delivery systems.[38,39] We envisioned that incorporating periodate-oxidized cholesterol-containing dextran (OCDEX) nanogels as drug carriers in a hydrogel would improve the formulation and make it more suitable for drug delivery. As a chemical crosslinker, the aldehyde group-bearing OCDEX nanogel should react with the amino-bearing polysaccharide/polypeptide

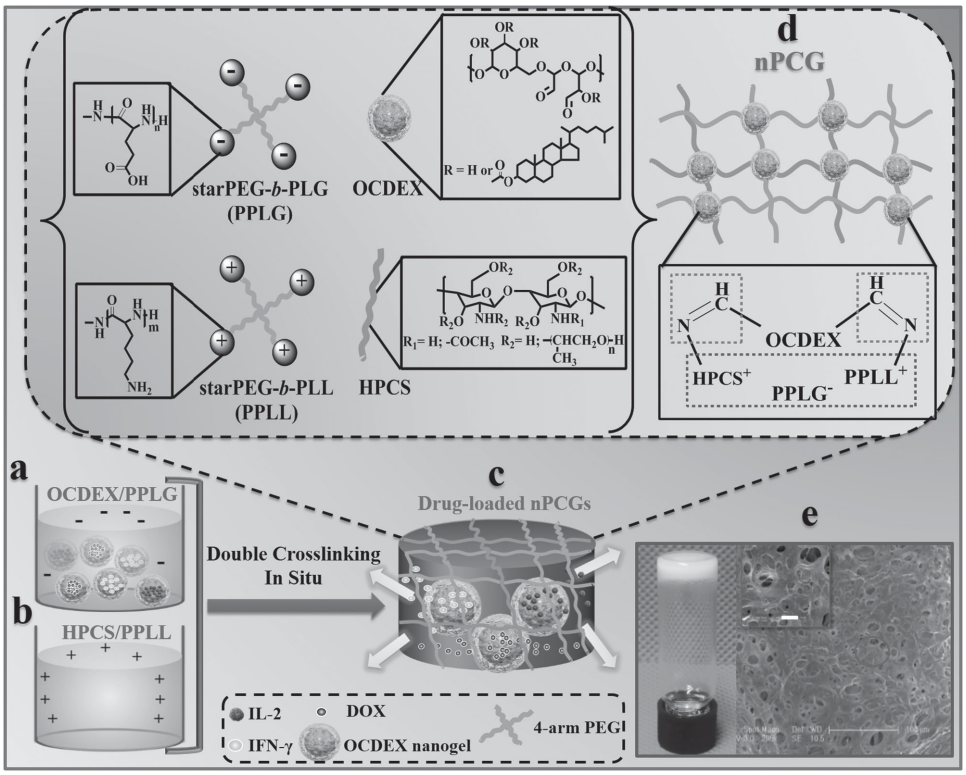

Figure 1. Schematic concept of a nanogel-incorporated physical and chemical gel (nPCG) as a delayed-release biosystem. a) Negatively charged mixtures of a drug-loaded oxidized cholesteryl-bearing dextran (OCDEX) nanogel solution containing 4-arm poly(ethylene glycol)-*b*-poly(L-glutamic acid) (PPLG) and b) positively charged complex hydroxypropyl chitosan/4-arm poly(ethylene glycol)-*b*-poly(L-lysine) (HPCS/PPLL) prepared in PBS at pH 7.4. c) Drug-loaded hydrogels were formulated by the ionic crosslinking of negatively charged PPLG with positively charged polysaccharide/polypeptide composites (HPCS/PPLL) and the simultaneous Schiff-base reaction between amino-containing HPCS/PPLL complexes and aldehyde group-bearing nanogels containing IL-2, IFN-γ and DOX. d) Schematic illustration for the formation of double-crosslinking networks of nPCG. e) Optical image showing that the fabricated dual-crosslinking nPCG is white and opaque. SEM images manifest that the micropores inside the hydrogel are all interconnected. Scale bar of the inset is 10 μm.

© 2015 WILEY-VCH Verlag GmbH & Co. KGaA, Weinheim

complex of hydroxypropyl chitosan (HPCS) and 4-arm poly(ethylene glycol)-*b*-poly(L-lysine) (PPLL) to form imine bonds. These imine bonds could potentially enhance the initial ionic crosslinking of the negatively charged 4-arm poly(ethylene glycol)-*b*-poly(L-glutamic acid) (PPLG) with the positively charged composites (HPCS/PPLL), resulting in the interpenetration of two different networks controlled by two distinctly different mechanisms and further enhanced gel network stability via network interdigitation. The nPCG system with incorporated protein agents (IL-2 and IFN-γ) and chemotherapeutic drug (DOX) demonstrates a significant synergistic effect for the treatment of A549 xenograft tumors compared to chemotherapy or protein therapy alone. The unprecedented nanogel-integrated hydrogel material with a double cross-linking structure for chemo-protein combination therapy represents a new class of local delivery carrier for cancer treatment.

2. Results and Discussion

2.1. Design of Nano-structured Physical and Chemical Composite Gels (nPCGs)

The nPCG systems were prepared by ionic interaction and Schiff base chemistry induced crosslinking reactions of sterile, filtered solutions containing the drug-loading OCDEX nanogels, the negatively charged PPLG, and the positively charged polysaccharide/polypeptide complex (HPCS/PPLL) in phosphate buffered saline (PBS) (Figure 1a–c). Figure S1 (Supporting Information) shows the synthesis of the four-arm, star-shaped block copolymers PPLG and PPLL through ring-opening polymerization (ROP) of the α-amino acid *N*-carboxyanhydride (NCA) monomers with 4-arm amino-functionalized PEG (4-arm PEG-NH_2) as a macroinitiator. Cholesteryl-bearing dextran (CDEX) was obtained by esterification of dextran with cholesteryl chloroformate, which was subsequently oxidized by $NaIO_4$ to obtain the OCDEX nanogels. HPCS was prepared from chitosan (CS) using propylene oxide as the etherifying agent and sodium hydroxide as the catalyst. The preparation of 4-arm PEG-NH_2, PPLG, PPLL, CDEX, OCDEX, and HPCS, as well as the chemical characterization of the prepared polymers, is provided in the Supporting Information (Figure S1 and S2). ^{1}H NMR studies were used to determine the degree of substitution (DS) of cholesterol (Supporting Information: Figure S2d,e). No NMR signals corresponding to cholesterol were found for OCDEX in D_2O (Supporting Information: Figure S2f), which confirmed the formation of self-assembled OCDEX nanogels in aqueous solution due to the restricted motions of the cholesterol protons within the formed hydrophobic micellar core. The OCDEX nanogels showed a narrow size distribution with a mean hydrodynamic radius of 228 ± 18.5 nm, based on the measurements by dynamic light scattering (DLS) and transmission electron microscopy (TEM) (**Figure 2**). Figure 1e shows the as-prepared dual-crosslinked nPCG, denoted as O_xG_y/H_zL_w, whereby the subscripts represent their respective concentrations (in mg mL^{-1}) in the gel. It can clearly be seen that the nPCG is slightly opaque. The gelation was completed within seconds for all nPCG formulations studied. Scanning electron microscopy (SEM) images (not shown) revealed that the microstructures of freeze-dried nPCGs ($O_3G_{64}/H_{20}L_{64}$) were highly porous with interconnected micropores ranging from 1 to 10 μm, which furnished efficient channels for drug transport.

The viscoelastic dynamic moduli of the varying hydrogel formulations were studied by rheological analysis (**Figure 3**a). Considering the cross-linking continued after mixing, the larger aggregates were formed with more compact structures and higher friction, which markedly enhanced the mechanical properties of the hydrogel.[40] Therefore, the elastic modulus (G') and viscous modulus (G'', see Figure S3a, Supporting Information) increased over time. Compared to gels formed by physical ($G_{64}/H_{20}L_{64}$) or chemical ($O_3/H_{20}L_{64}$) crosslinking alone, the double-network structure of $O_3G_{64}/H_{20}L_{64}$ was much more rigid with a G' of around 4 400 Pa. With increasing concentration of the nanogel cross-linking agent (OCDEX), the rigidity of the nPCGs also increased further and the highest rigidity was obtained for the composite material $O_{12}G_{64}/H_{20}L_{64}$, which showed a threefold increase (G' of ca. 13 800 Pa). Such drastically increased rigidity may be attributed to the formation of the double networks, first through ionic crosslinking followed by a covalent crosslinking induced by a Schiff-base conjugation reaction between the aldehyde group-containing OCDEX nanogels and the amino-bearing compounds (HPCS/PPLL). The strength of this double network is in sharp contrast to that of a single crosslinking network, which could only be tuned at

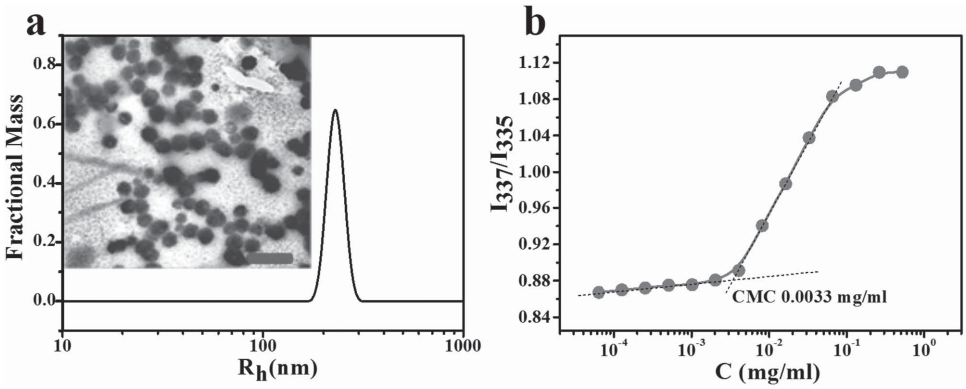

Figure 2. a) Hydrodynamic radius distribution and morphology of OCDEX nanogels in aqueous solution as determined by DLS and TEM (scale bar: 500 nm). b) Critical micelle concentration (CMC) of OCDEX nanogels.

© 2015 WILEY-VCH Verlag GmbH & Co. KGaA, Weinheim

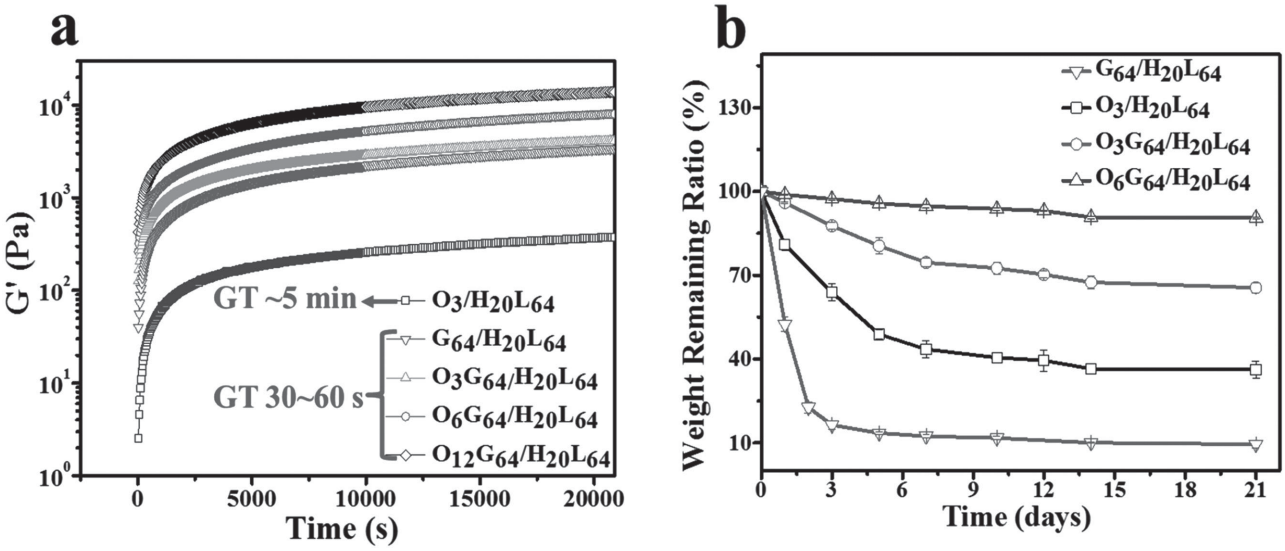

Figure 3. Mechanical properties and in vitro degradation of nPCGs. a) Rheological analysis showing the elastic modulus (G') as a function of time for different hydrogel formulations (O_xG_y/H_zL_w). The subscripts x, y, z, and w represent their respective concentrations (mg mL^{1}) in the gel. The gelation time is designated as GT. b) The effect of single or double crosslinking on degradability in PBS at pH 7.4 and 37 °C. Results are shown as the average values ± S.D. ($n = 3$).

much lower G' (from 400 to 5 300 Pa) by varying the concentration (Figure S3b,c, Supporting Information). The degradation of the composite hydrogels was evaluated as a function of incubation time in PBS (Figure 3b). Compared to $O_3/H_{20}L_{64}$ and $G_{64}/H_{20}L_{64}$, the double crosslinking hydrogels ($O_3G_{64}/H_{20}L_{64}$ and $O_6G_{64}/H_{20}L_{64}$) showed much lower weight loss rates and a markedly enhanced stability. Only 10% mass loss was observed for the $O_6G_{64}/L_{64}H_{20}$ group after 21 days of the degradation experiment. $O_{12}G_{64}/H_{20}L_{64}$ showed no obvious degradation over one month with a total mass loss below 3% (data not shown). These results, taken together, suggest that, in spite of the weaker ionic crosslinking, the strength and stability of the gels could be observably enhanced by a Schiff base reaction between the aldehyde group-containing nanogels and amino-bearing HPCS/PPLL complex.

2.2. In vitro Synergistic Cytotoxicity and Cell Apoptosis

We hypothesized that the introduction of drug-loaded OCDEX nanogels as nano-crosslinkers in a hydrogel could result in well-preserved activities of the contained drugs and simultaneously bring about the sustained release of these agents. To accomplish this, the release of IL-2, IFN-γ, and DOX from nPCGs was explored in PBS using OCDEX nanogels as the control (Figure S4, Supporting Information). Our drug-loaded nPCGs appeared to display a similar biphasic release pattern for all three substances, characterized by a first rapid release followed by a slower and sustained release. For all contained agents in nPCGs, the corresponding release rate was found to be significantly lower than that from OCDEX, which could be attributed to the formation of the nanogel-incorporated hydrogel. Moreover, the electrostatic interactions between the drugs and the nanogel/hydrogel hybrid networks may also result in a slower delivery rate.

The in vitro antitumor activities of drugs from the nPCGs were evaluated using three different human tumor cell lines: A549, HeLa, and MCF-7 (**Figure 4**a). The hydrogel matrices showed no detectable toxicity against these cells with viabilities ranging from 91.4 to 95.7%. The treatment with IL-2/IFN-γ/DOX-loaded nPCGs resulted in significantly lowered viabilities than that for the gel+IL-2/IFN-γ or gel+DOX treatments alone. The survival percentage after 96 h for A549 cells treated with nPCGs containing 3.24×10^5 IU mL^{-1} IL-2 plus 2.28×10^5 IU mL^{-1} IFN-γ was 56.7%, and the survival of cells treated with nPCGs containing 34.0 μg mL^{-1} DOX was 38.6%. However, the viability was significantly reduced to 21.1% for the cells treated with nPCGs containing IL-2/IFN-γ/DOX at the aforementioned concentrations. Similar results were also observed in HeLa and MCF-7 cells, substantiating that the benefit of the combination of chemotherapeutics and protein (IL-2, IFN-γ, and DOX) was more effective than either treatment alone in inducing cell death in A549, HeLa, and MCF-7 cells. The cytotoxicities of the free drug solutions were also evaluated after incubation at different times (Figure S5, Supporting Information). After 96 h of incubation, the drug-loaded nPCGs revealed a slightly lower toxicity as compared to equal amounts of the free agents. The gel+IL-2/IFN-γ/DOX and free IL-2/IFN-γ/DOX treated A549 cells were also analyzed by flow cytometry (Figure 4b). The 7-AAD^- annexin V^+ cells and 7-AAD^+ annexin V^+ cells were defined as apoptotic/necrotic cells. The results showed that a higher ratio of apoptotic/necrotic cells and lower ratio of normal cells were obtained for gel+IL-2/IFN-γ/DOX and free IL-2/IFN-γ/DOX after incubation for 96 h compared to that for the single treatments . The data in Figure 4a,b suggest that the cytotoxic effect of DOX on tumor cells is promoted by the protein agents (IL-2/IFN-γ), which further confirms the synergistic antitumor effect induced by IL-2/IFN-γ/DOX in the nPCGs.

© 2015 WILEY-VCH Verlag GmbH & Co. KGaA, Weinheim

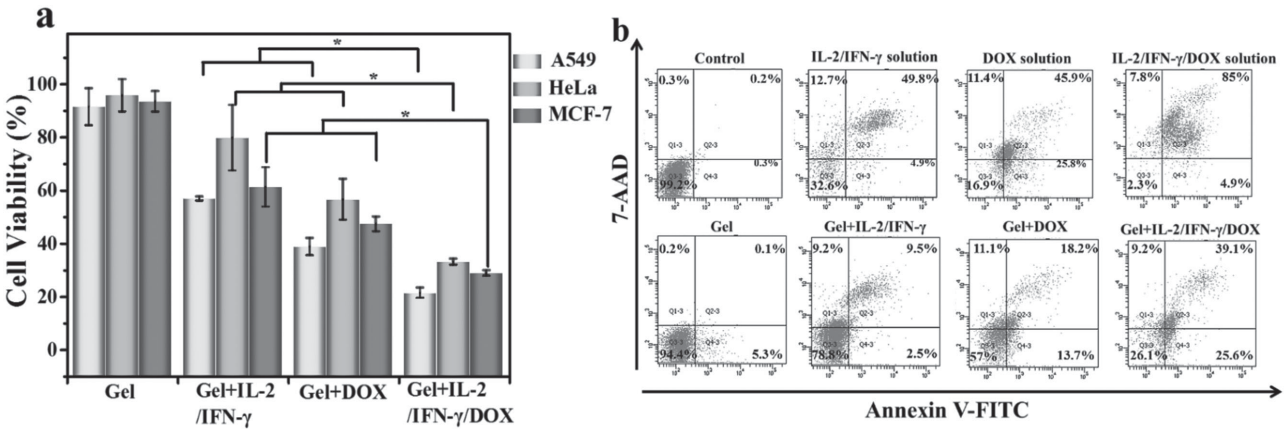

Figure 4. Inhibition of tumor cell proliferation and induction of apoptosis upon treatment with IL-2/IFN-γ/DOX-incorporated nPCGs. a) The viability of A549, HeLa, and MCF-7 cells measured by a tetrazolium-based colorimetric assay after 96-hour treatment with IL-2/IFN-γ/DOX-loaded nPCGs. b) Flow cytometry analysis of A549 cell apoptosis induced by different formulations for 96 h by using Annexin V-FITC/7-AAD staining. $*P < 0.05$.

2.3. In vivo Kinetics of Drug Release

The plasma pharmacokinetics were investigated by administering a free IL-2/IFN-γ/DOX solution and IL-2/IFN-γ/DOX loaded nPCGs subcutaneously into mice (**Figure 5**). At 1 h post injection, the high concentrations of IL-2, IFN-γ, and DOX in the plasma of mice treated with drug solution confirmed that the injected agents entered the bloodstream rapidly. In contrast, the concentrations of drugs in the plasma of mice treated with gel+IL-2/IFN-γ/DOX were much lower. From 1 to 3 h post injection, the concentrations of IL-2, IFN-γ, and DOX in the plasma treated with drug solution decreased rapidly and continuously to 121, 174, and 75 000 pg mL^{-1}, respectively, at 6 h post injection. However, the corresponding drug concentrations for IL-2/IFN-γ/DOX loaded nPCGs-treated mice were 465, 532, and 278 000 pg mL^{-1}, indicating a more sustained drug release from nPCGs. The percentages of agent delivered at the tumor site were further explored (see insets in Figure 5a,b). At 10 h post injection, the delivered amounts of IL-2 and IFN-γ at the tumor site of drug-loaded nPCGs-treated mice were 3620 and 2930 pg g^{-1} of tumor tissue, respectively, both of which were approximately three times higher than the amounts for the mice treated with the free drug. The delivered amount of DOX in the drug-containing gel-treated mice was five-fold of the amount in the mice treated with the free drug. Thus, the nPCGs provided a markedly improved delivery of the drugs at the tumor site when compared to free drug injection.

2.4. Synergistic Antitumor Activities in Tumor-Xenografted Nude Mice

To investigate the anti-tumor efficacy of drug-incorporated nPCGs in vivo, BALB/c nude mice bearing human non-small-cell lung cancer (A549) were treated by a single peritumoral injection of PBS, gel, free IL-2/IFN-γ/DOX, gel+IL-2/IFN-γ, gel+DOX, or gel+IL-2/IFN-γ/DOX. The tumor growth was not inhibited in the PBS group and the gel-treated group, and the tumor sizes increased rapidly during the treatment period of 21 d (**Figure 6**a,b). In contrast, the tumor growth was

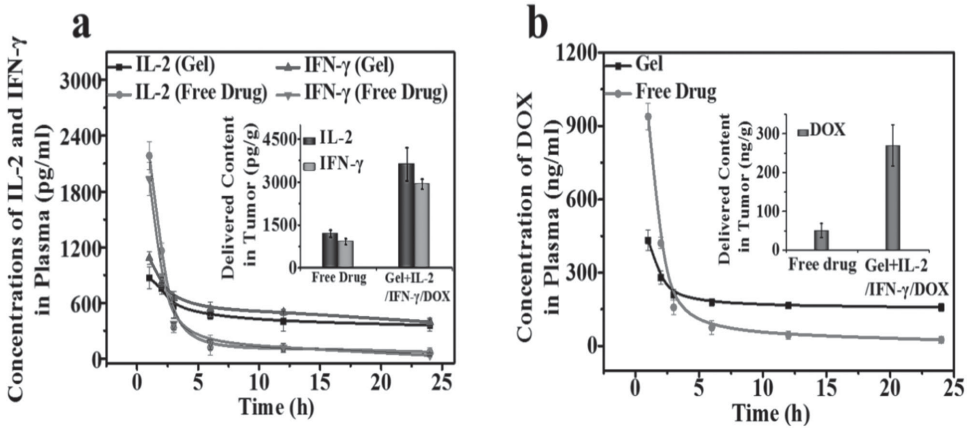

Figure 5. Pharmacokinetics of IL-2, IFN-γ, and DOX in the plasma and delivered drugs in the tumor of mice. Pharmacokinetics curves for a) IL-2, IFN-γ and b) DOX in the plasma of BALB/c nude mice. The insets in (a) and (b) show amounts of IL-2, IFN-γ, and DOX delivered to tumor tissues of A549 inoculated BALB/c nude mice at 10 h post injection. The amounts of IL-2, IFN-γ (pg), and DOX (ng) delivered at the tumor tissue were normalized to the weight of the tumor (g). Data are presented as a mean ± S.D. ($n = 5$).

© 2015 WILEY-VCH Verlag GmbH & Co. KGaA, Weinheim

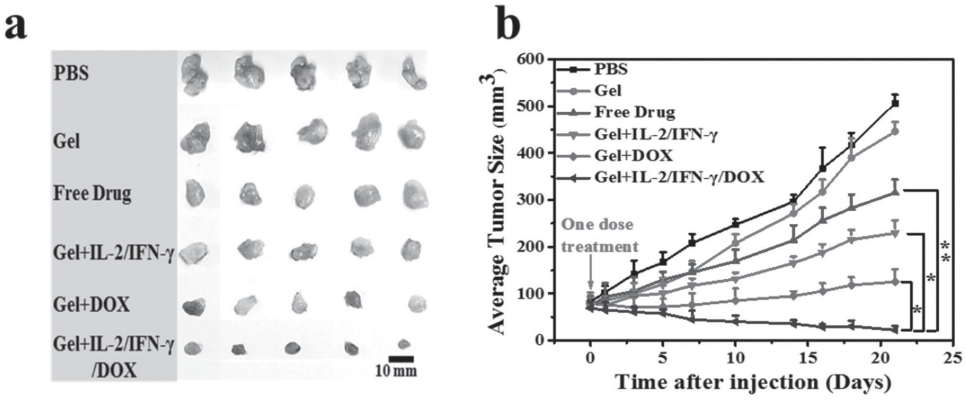

Figure 6. Tumor regression study of A549-inoculated BALB/c nude mice treated with different formulations. a) Gross solid tumor images of mice injected subcutaneously with different formulations at 21 days post treatment. b) Tumor sizes of the mice as a function of time. The arrows represent the day on which the subcutaneous injection was performed ($n = 5$). $^{*}P < 0.05$. $^{**}P < 0.01$.

clearly inhibited in all of the other groups (treated with free IL-2/IFN-γ/DOX, or the IL-2/IFN-γ/DOX-loaded formulations). The drug-containing nPCGs showed a significant decrease in the average tumor size due to the prolonged retention time of IL-2, IFN-γ, and DOX at the tumor site and the synergistic anticancer effect of the chemo-biological therapy. The mice treated with all hydrogel formulations maintained their body weights and were alive throughout the study period. However, the body weights of mice receiving free IL-2/IFN-γ/DOX solution reduced during the treatment ($P < 0.05$) (Figure S6, Supporting Information). These results indicated that the drugs contained in nPCGs showed a lower toxicity to normal cells. Collectively, the data suggested that the combination treatment of IL-2, IFN-γ, and DOX attained a remarkable anticancer efficacy in lung-cancer bearing mice, resulting in satisfactory survival rates.

2.5. Histological and Immunohistochemical Analyses

Hematoxylin and eosin (H&E) staining assays were used next to evaluate the histological features of the tumors and the major organs (heart, liver, spleen, lung, and kidney). As shown in **Figure 7**a, dense tumor cells were observed in the tumor tissue

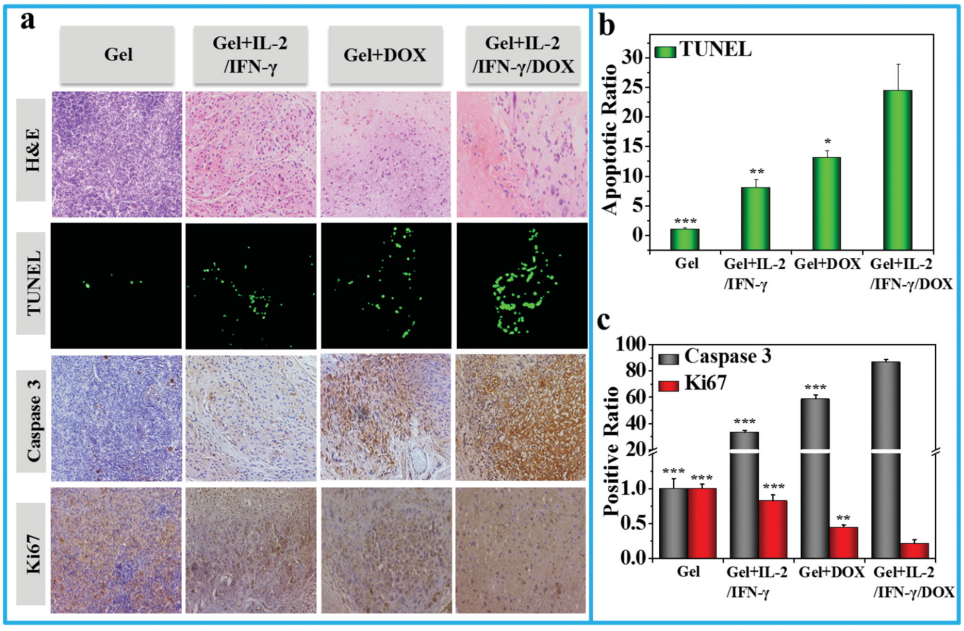

Figure 7. Ex vivo histological, TUNEL, and immunohistochemical analyses of A549 tumor sections (21 days after the first treatment). a) Hematoxylin and eosin (H&E), immunohistochemical staining for apoptotic cells (TUNEL and Caspase 3), and proliferating cells (Ki-67 staining) of lung tumors treated with different formulations. More Caspase 3 positive cells in tumor tissues were observed in the gel+IL-2/IFN-γ/DOX group. The tumor cells of blank gel-treated mice displayed a significantly intense positive staining for Ki-67. b,c) Quantification of (a). The number of TUNEL positive cells in the gel+IL-2/IFN-γ/DOX group was significantly higher than in the gel+IL-2/IFN-γ ($p < 0.01$), gel+DOX ($p < 0.05$), or blank gel ($p < 0.001$) group. Ki-67 staining revealed a significant decrease of positive cells in tumor sections of the mice treated with gel+IL-2/IFN-γ/DOX as compared to the gel+IL-2/IFN-γ ($p < 0.001$), gel+DOX ($p < 0.01$), and gel ($p < 0.001$) groups. In contrast, the tumor cells were highly proliferative in the group treated with blank gel. Values represent mean ± S.D. ($n = 3$).

© 2015 WILEY-VCH Verlag GmbH & Co. KGaA, Weinheim

treated with empty nPCGs, indicating a rapid tumor growth. The groups treated with gel+IL-2/IFN-γ or gel+DOX displayed relatively lower necrotic levels, whereas those treated with gel+IL-2/IFN-γ/DOX exhibited the largest necrosis area. The intracellular markers of apoptosis and proliferation in the tumor sections of all groups were determined by terminal deoxynucleotidyl transferase dUTP nick-end labeling (TUNEL) and immunohistochemical analysis. TUNEL staining (green) on tumor cross sections was performed to assess the effect of various nPCGs formulations on the apoptosis in tumors by visualizing a marker of late apoptosis. Tumors treated with gel+IL-2/IFN-γ/DOX resulted in the highest green fluorescence intensity, which is thus associated with the highest apoptosis level of tumor cells. TUNEL-positive cells were counted quantitatively and the apoptosis ratio is shown in Figure 7b. Activated Caspase 3 is evidently indispensable for programmed cell death (apoptosis), because of its mediation in the limited proteolysis of key substrate proteins and the cleavage inactivation of DNA fragmentation factors.[41] The tumor cells of gel+IL-2/IFN-γ/DOX-treated mice displayed significantly intense positive staining for Caspase 3. Ki-67 is a nuclear protein strictly associated with cell proliferation.[42] Ki-67 staining revealed a significant decrease of positive cells in the tumor sections of the mice treated with gel+IL-2/IFN-γ/DOX as compared to the other groups. Taken together, the data in Figure 7b,c indicate that the IL-2/IFN-γ/DOX loaded nPCGs-treated group showed a more pronounced apoptosis.

2.6. Mechanisms of Synergistic Antitumor Effects

To better understand the collaborative anti-tumor mechanisms of IL-2/IFN-γ/DOX in nPCGs, the relevant gene expressions were analyzed in distinct signaling pathways (**Figure 8**). The physiological cell death process of apoptosis is a programmed counterbalance to mitosis.[43] Data from in vivo studies suggest that IL-2/IFN-γ/DOX-induced apoptosis involves an IL-2/IFN-γ activated JAK-STAT pathway and DOX-mediated mitochondrial signaling pathway (**Figure 9**). Several key apoptosis-regulating genes involving STAT5, STAT1, Caspase 9, Bax, Caspase 3, and Bcl-2, have been evaluated in tumor tissues. The binding of cytokines to cytoplasmic membrane receptors by receptor–ligand interactions has been performed to show the existence of receptor-mediated downstream signal transduction pathways.[44] JAKs are protein tyrosine kinases that play a pivotal signaling function for the downstreaming of cytokine receptors.[45] IL-2 stimulation promotes tyrosine phosphorylation of JAK1 and JAK3 through interactions with its receptors (IL-2Rβ and IL-2Rγ), and further induces significant tyrosine phosphorylation of STAT5[46] (a member of the signal transducer and activator of transcription, STAT, family). After the formation of a STAT5 homodimer, the activated STAT5 dimer is to enter the nucleus and activate the expressions of the backward anti-apoptosis genes (Bcl-2 and Bcl-xl).[47] However, the interaction between IFN-γ and its receptors (IFN-γR1 and IFN-γR2) at the plasma membrane can separately give rise to the activation of JAK1 and JAK2, which ultimately phosphorylate the substrate proteins called STAT1.[48] The dimerization of phosphorylated STAT1 can then be followed by translocation to the nucleus, binding of specific DNA chains, and directing transcription to up-regulate apoptosis genes (Caspase 3 and Caspas-8).[49] As shown in Figure 8a,b, the expression of STAT5 upstream of the Bcl-2 gene in the groups treated with gel+IL-2/IFN-γ/DOX or gel+IL-2/IFN-γ was significantly reduced, whereas the expression of STAT1 upstream of the Caspase 3 gene had increased

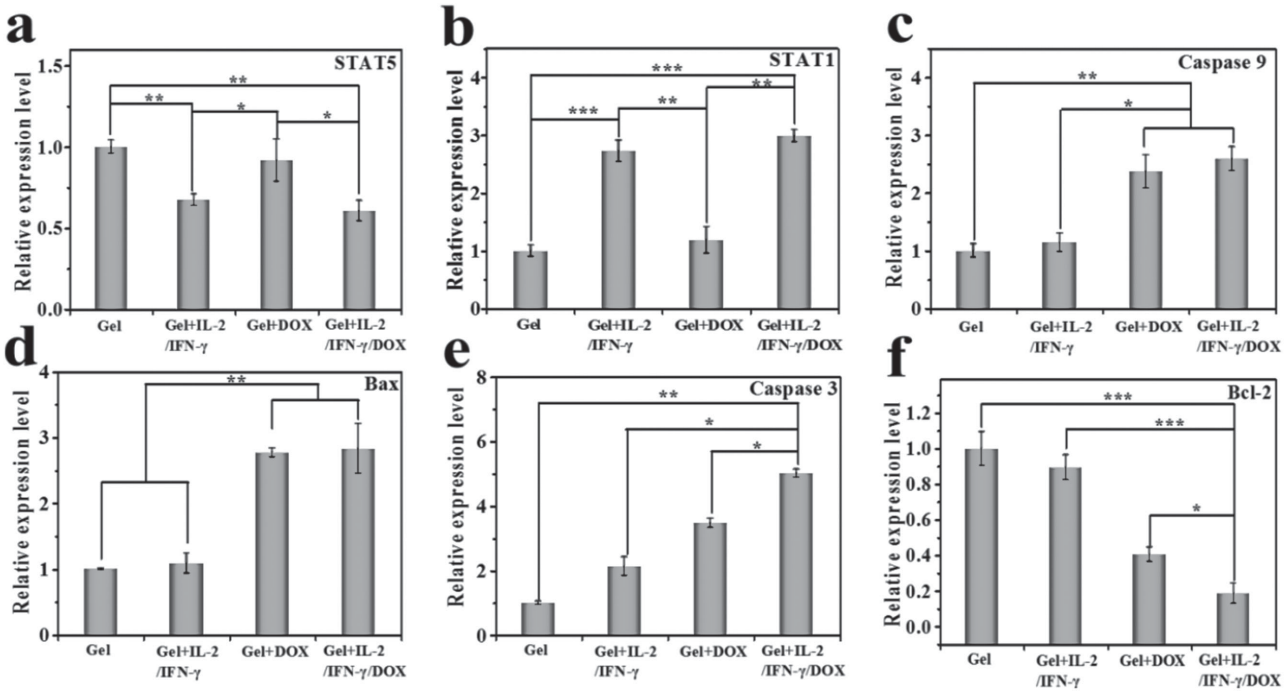

Figure 8. The expressions of apoptosis-related genes in tumor tissues analyzed by quantitative real-time PCR (qPCR). a) STAT5, b) STAT1, c) Caspase 9, d) Bax, e) Caspase 3, f) Bcl-2. $^{*}P < 0.05$. $^{**}P < 0.01$. $^{***}P < 0.001$.

© 2015 WILEY-VCH Verlag GmbH & Co. KGaA, Weinheim

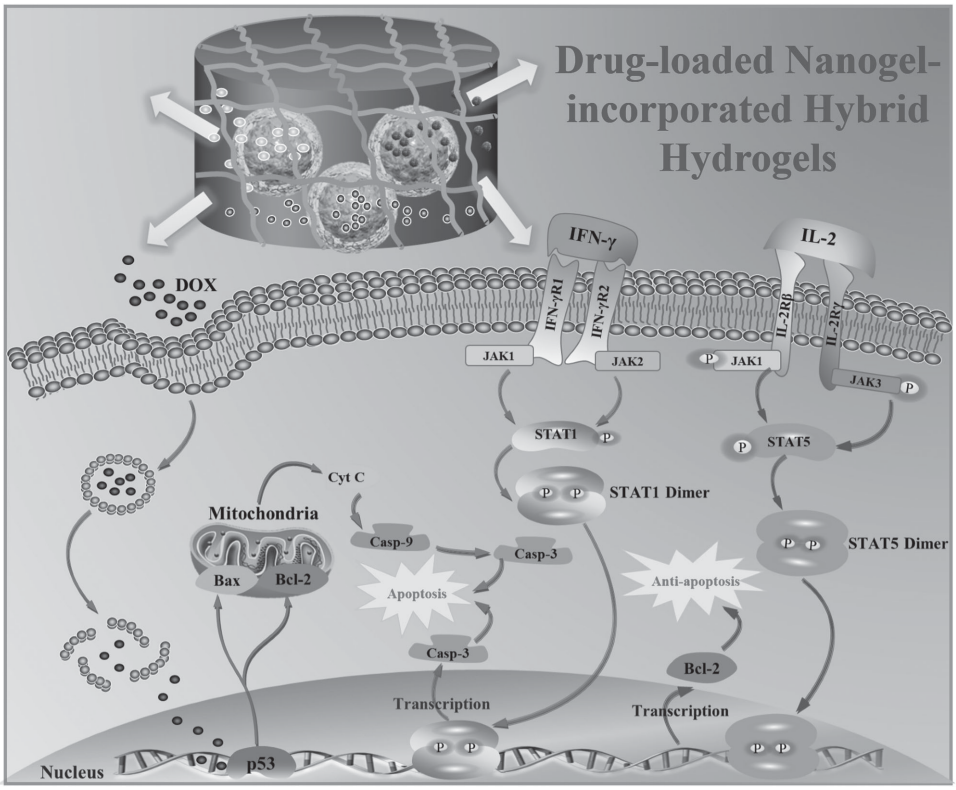

Figure 9. Simultaneous delivery of IL-2/IFN-γ to the cytolemma and DOX to the nuclei by IL-2/IFN-γ/DOX-loaded nPCGs for combination cancer treatment. The IL-2/IFN-γ/DOX-induced apoptosis involves an IL-2/IFN-γ activated JAK/STAT pathway and a DOX mediated mitochondrial signaling pathway including several key apoptosis-regulating genes such as STAT5, STAT1, Caspase 9, Bax, Caspase 3, and Bcl-2.

compared to that in blank gel or gel+DOX groups. Thus, the results suggest that the IL-2/IFN-γ-mediated JAK-STAT pathways could indeed be inducing apoptosis as a result of the regulating activation of downstream apoptotic/anti-apoptotic genes.

Activation of p53 plays a crucial role in DOX-induced tumor cell apoptosis.[50,51] Accumulation of p53 can induce the up-regulation of pro-apoptotic members of the Bcl family, for instance, Bax and Puma, and/or the down-regulation of anti-apoptotic Bcl proteins,[52] such as Bcl-2 and Bcl-xl. Synchronously, p53 can also affect mitochondria to release cytochrome C (Cyt C), which can further active pro-Casp 9 and trigger the sequential activation of the apoptosis executioner Caspase 3.[52,53] Caspase 3 activation has been shown to play an important role in apoptotic induction of human cancers, such as breast and colon cancer.[41] The expressions of Caspase 9 and Bax (Figure 8c,d) in the group of mice treated with gel+IL-2/IFN-γ/DOX or gel+DOX were both remarkably higher than those in the groups treated with blank gel or gel+IL-2/IFN-γ, indicating that Caspase 9 and Bax are necessary for the DOX-induced pathway of apoptosis. Figure 8e,f revealed a significant increase in Caspase 3 expression and a decrease in Bcl-2 level in the tumor tissues of the group of mice treated with gel+IL-2/IFN-γ/DOX compared to that in the other groups. The data suggest that the expressions of the apoptosis gene (Caspase 3) and anti-apoptosis gene (Bcl-2) in tumors treated with IL-2/IFN-γ/DOX loaded nPCGs were jointly regulated by JAK-STAT and mitochondrial pathways with p53, STAT5, and STAT1 as the important upstream factors. Thus, these results validate the synergistic mechanism of our chemo-protein therapy in inducing the apoptosis/death of A549 human lung adenocarcinoma cells and suppressing tumor growth in vivo.

2.7. Discussion

The current study presents a novel, double-crosslinking strategy for the development of nanostructured hybrid hydrogels with enhanced mechanical stability, sustained drug release profiles, and desired biodegradability. Fast gelation (within seconds) was attributed to the ionic crosslinking of negatively charged PPLG with positively charged polysaccharide/polypeptide complex (HPCS/PPLL) and the simultaneous Schiff-base reaction between aldehyde group-containing OCDEX nanogels and amino-bearing HPCS/PPLL compounds. The formulation of the nanostructured architecture was designed to improve the kinetic release profiles of multiple drugs by offering a nanoscale reservoir barrier to moderate or remove the burst release effects of drugs in injectable formulations. The IL-2/IFN-γ/DOX-loaded nPCGs therapy with a single-dose treatment displayed the highest efficiency in tumor suppression and caused less toxic side effects in vivo (Figure S7, Supporting Information). These results could be attributed to the prolonged and continuous release at the tumor site of the agents encapsulated in nPCGs. IL-2 and IFN-γ are important cytokines that can activate cytolytic T-lymphocytes ($CD8^+$ T cells) to kill tumor cells.[14,54] Our study suggests that IL-2 and IFN-γ produced cooperative cytostatic and cytocidal effects directly on tumor cells by activating

© 2015 WILEY-VCH Verlag GmbH & Co. KGaA, Weinheim

different apoptosis signal pathways. Moreover, the tumor cytotoxicity of the protein therapeutics was further enhanced by using a chemotherapeutic agent (DOX), thus involving the combined effects of three different apoptosis-related JAK/STAT and mitochondrial pathways. In the JAK/STAT pathway, STAT5 and STAT1 are considered to be key regulators to the downstream signaling pathway and cell apoptosis through binding specific DNA fragments and activating the transcriptional expression of anti-apoptosis genes (e.g., Bcl-2) and apoptosis genes (e.g., Caspase 3). The mitochondria-mediated apoptosis pathway involves p53, Bcl proteins, and Caspases. Accumulation of p53, triggered by DOX, can induce the up-regulation of pro-apoptotic proteins (Bax, Caspase 9, Caspase 3, etc.) and/or the down-regulation of anti-apoptotic proteins (Bcl-2). Thus, the combination of IL-2/IFN-γ/DOX observably increased the expression of the pro-apoptosis gene (Caspase 3), while it decreased the expression of the anti-apoptosis gene (Bcl-2) significantly. The synergistic anticancer effect of nPCGs-based chemo- and protein therapy was thus a result of the modulation of distinct apoptosis-related genes.

3. Conclusions

We successfully developed well-defined syringe-injectable nanogel-crosslinked physical and chemical composite gels (nPCGs) that could simultaneously deliver IL-2, IFN-γ, and DOX to tumor regions for combined chemo-protein therapy. This double-network formulation not only increased the stability of the protein agents, but it also extended the drug release, which enhanced intratumoral drug enrichment and decreased drug-related multi-organ damaging. The combination treatment of drug-loaded nPCGs had a significant tumor inhibition effect in the nude mouse models with transplanted subcutaneously tumor based on the A549 cell line. Hence, these features substantiate the prospective merit of this scheme for combined chemo-protein therapy. Further research using such delayed-release systems for cytokines-mediated immunotherapy in combination with DOX chemotherapy is currently underway in orthotopically transplanted breast and colon mice tumor models, which is expected to achieve superior therapeutic effects. The strategy can be expanded to formulate various types of drug-containing hydrogels by using multiple drug-loaded nanogels as crosslinkers for a wide range of applications including long-term drug-delivery systems, microbioreactors, and 3D scaffolds for tissue engineering.

4. Experimental Section

Materials: Dextran (from Leuconostoc spp., M_w = 100 000), chitosan (deacetylation degree 85%, low molecular weight), sodium periodate, and the nitrite/nitrate assay kit were purchased from Sigma-Aldrich. 4-arm Poly(ethylene glycol) (4-arm PEG) (M_w ca. 10000) and *N*-(tert-butoxycarbonyl)-L-phenylalanine were obtained from Jenkem Technology Co., Ltd. Doxorubicin hydrochloride (DOX) was supplied by Beijing Huafeng United Technology Corp. (Beijing, P. R. China). Recombinant human Interleukin-2 (IL-2, specific activity 3.0×10^7 IU mg^{-1}) and recombinant human Interferon Gamma (IFN-γ, specific activity 2.0×10^7 IU mg^{-1}) (Cloud-Clone Corp., USA) were used as obtained without purification. Chloroform, dimethyl sulfoxide (DMSO), dichloromethane (DCM), and *N*,*N*-dimethylformamide (DMF) were stored over calcium hydride (CaH_2) and distilled under nitrogen. All the other reagents and solvents were of the highest purity available.

Fabrication of OCDEX Nanogels: The self-assembled nanogels were obtained by dissolving the lyophilized OCDEX in phosphate buffered saline (PBS) (pH 7.4). The hydrodynamic diameter distribution of the amphiphilic OCDEX nanogels in water at 25 °C were measured by Wyatt QELS (Wyatt Technology Corp.). Transmission electron microscopy (TEM, FEI Tecnai G2 20) was used to observe the morphologies of the OCDEX nanogels in the dry state at an acceleration voltage of 200 kV. The critical micelle concentration (CMC) of the OCDEX nanogel was determined by fluorescence spectroscopy using pyrene as the fluorescence probe. The nanogel/IL-2, nanogel/IFN-γ, and nanogel/DOX complexes were separately formed by dissolving IL-2, IFN-γ, and DOX in PBS, pH 7.4 (the pH of the nanogel/DOX solution was adjusted to 7.4 with triethylamine), followed by dissolution of lyophilized OCDEX, for approximately 12 h at 25 °C under stirring. The excess drug was removed by ultrafiltration using an Amicon Ultra-15 device at 100 kDa (Millipore Corp.), to elute the unbound proteins and DOX. For determination of the drug-loading efficiency (DLE) and drug-loading content (DLC), the free IL-2 and IFN-γ in solution were analyzed using an ELISA commercial kit in order to evaluate the amount of IL-2 and IFN-γ incorporated. The loading of DOX was determined by quantifying the amount of free DOX in solution by fluorescence spectroscopy (Perkin-Elmer LS50B luminescence spectrometer) using a standard curve method. The DLC and DLE were calculated according to the following formulae:

$$\mathrm{DLE}\,(\mathrm{wt.\%}) = \frac{\text{weight of loaded drug}}{\text{weight of fed drug}} \times 100\% \quad (1)$$

$$\mathrm{DLC}\,(\mathrm{wt.\%}) = \frac{\text{weight of loaded drug}}{\text{weight of drug} - \text{loaded nanogel}} \times 100\% \quad (2)$$

Physicochemical Characterizations of nPCGs: Rheological measurements of the nPCGs were performed on a Anton Poar Physica MCR 301 rheometer using a parallel plate (plate diameter = 25 mm, gap = 0.5 mm) in oscillatory mode at 37 °C. For the measurements, hydrogel samples were prepared on the plate of the instrument immediately. We conducted dynamic time sweeps on nPCG samples under various conditions. The elastic modulus (G') and viscous modulus (G'') were recorded at 10 percent of strain and a frequency of 1 Hz. The sample was sealed by a thin layer of silicon oil to prevent it from drying out.

The in vitro degradation of the hydrogel samples was determined by gravimetry. nPCGs (200 μL) were fabricated in microtubes and subsequently immersed in 2 mL of PBS at 37 °C. At pre-determined time intervals, the weight of the degraded hydrogels was measured after removal of the media from the microtubes. The remaining weight% of the hydrogels was then calculated according to the following equation:

$$\text{Weight remaining percentage of hydrogel (\%)} = (W_t / W_0) \times 100\% \quad (3)$$

where W_t is the dry weight of the degraded hydrogels at different time intervals and W_0 is the weight of the initial hydrogels.

Design of nPCGs for co-Delivery of IL-2, IFN-γ, and DOX: The fabrication of drug-incorporated nPCGs is presented in Figure 1a-c. Briefly, the drug-loaded nanogels were first prepared in a PBS solution (pH 7.4), which contained a DOX/nanogel (feed ratio of 0.3, DLE = 96.2%, DLC = 22.1%), IL-2/nanogel (feed ratio of 0.1, DLE = 98.4%, DLC = 8.3%), and IFN-γ/nanogel (feed ratio of 0.1, DLE = 99.0%, DLC = 8.7%) with total nanogel concentrations of 6.0–24.0 mg mL^{-1}. Then, a PPLG amount of 32 mg, 64 mg, or 128 mg was added into 1.0 mL of prepared nanogel solution. As a result, drug-loaded nanogel solutions containing PPLG were prepared (solution a). Second, 1.0 mL PBS solutions containing HPCS at a fixed concentration of 40 mg mL^{-1} and PPLL with concentrations identical to PPLG were prepared (solution b). Solutions a and b were mixed in an equal volume ratio and vigorously stirred until the cross-linking reaction was

© 2015 WILEY-VCH Verlag GmbH & Co. KGaA, Weinheim

complete to obtain drug-loaded nPCGs. A constant HPCS concentration in the sol was chosen to yield a satisfactory fluidity and injectability and achieved by modifying the viscosity. The gelation time of nPCGs was assessed as the time at which no more flow could be observed. The micro-appearance of the hydrogels in the freeze-dried state was examined using field-emission scanning electron microscopy (SEM, Philips XL 30, 10 kV).

Release of IL-2, IFN-γ, and DOX from nPCGs in vitro and Bioactivity Analysis: 50 μL of IL-2/IFN-γ/DOX-incorporated nPCGs were prepared in each well of a 24-well Transwell insert chamber (Corning) perforated with 0.4-μm pores to allow media to flow freely into the wells of an underlying 24-well plate. 1 mL of PBS with 0.5% bovine serum albumin (BSA) were added to each chamber, which was incubated at 37 °C. At selected time points, the media was completely withdrawn and replaced with an equal volume of fresh buffer solution to maintain a constant total volume. The collected samples were stored in 2 mL Eppendorf Protein LoBind tubes at 4 °C until measurements. The protein concentrations were determined using a Human ELISA Kit for Interleukin 2 and a Human ELISA Kit for Interferon Gamma (Cloud-Clone Corp., USA). The concentrations of DOX in the above samples were determined by high-performance liquid chromatography (HPLC) (Waters e2695, USA) equipped with a fluorescence detector (Waters 2475, USA) using a standard-curve methodology (λ_{ex} 492 nm).

In order to avoid mutual interference of the drugs, the biological activity of the released protein agents (IL-2 and IFN-γ) were further assessed in mono-loaded formulations (gel+IL-2 and gel+IFN-γ) by quantifying the relative activities on IL-2-dependent murine (C57BL/6) cytotoxic T-cell line CTLL-2[55] and the amount of nitric oxide (NO) produced by the MH-S cells in response to IFN-γ.[56] The results are reported as a percentage of the activity achieved by the same mass of freshly reconstituted proteins (both IL-2 and IFN-γ over 91% for 14 days), confirming that the activity of the proteins was well maintained in the hydrogels.

Delivery of IL-2, IFN-γ, and DOX from nPCGs to Different Tumor Cell Lines in vitro: Three kinds of malignant human tumor cell lines, namely A549, HeLa and MCF-7 (from American Type Culture Collection, ATCC), which were derived from different tissues, were all maintained in Dulbecco's modified Eagle's medium (DMEM) supplemented with 10% fetal bovine serum (FBS). For each cell type, a 500 μL cell suspension containing 20 000 cells was added into each well of the 24-well plate and incubated for 24 hours before treatment. 50 μL of the nPCGs was added into each of the 24-well Transwell inserts and the drug-loaded nPCGs-containing inserts were then placed into the wells. Additionally, 500 μL of culture medium was added into the insert. After incubation for 96 hours at 37 °C, the cell viability was assessed using a tetrazolium salt (WST-8)-based colorimetric assay. The results were expressed as the percentage of the viability compared to that of untreated cells. In contrast, the cytocompatibility of the free drug solution with the same mass as the release media mentioned above was also studied for various incubation times (Figure S5a-c, Supporting Information). The analysis of apoptosis/necrosis on A549 after 4 days of culturing was carried out with an Annexin V-FITC Apoptosis Detection Kit (Roche Molecular Biochemicals), according to the manufacturer's instructions. The A549 cells were doubly stained with Annexin V and 7-AAD (BD Biosciences), and then sorted by flow cytometry (FCM, Beckman Coulter). The results are presented as the percentage of late apoptotic/necrotic (annexin V positive and 7-AAD positive), early apoptotic (annexin V positive and 7-AAD negative) and viable (annexin V negative and 7-AAD negative) cells.

Pharmacokinetics and Delivery of Drugs at Tumor Site: The IL-2/IFN-γ/DOX-loaded nPCGs and free IL-2/IFN-γ/DOX solutions were subcutaneously injected into the right anterior limb of five-week-old male BALB/c nude mice. At defined time periods (1 h, 2 h, 3 h, 6 h, 12 h, 24 h), blood samples from the tail vein were collected in heparinized tubes and centrifuged to obtain the plasma. The supernatant of each plasma sample was then taken and stored at –20 °C before measurements. To quantify the delivered amounts of agent at the tumor site, two groups of mice (n = 5) bearing A549 inoculated tumors with similar sizes were treated respectively with IL-2/IFN-γ/DOX-loaded nPCGs and free IL-2/IFN-γ/DOX solution. Then the mice were sacrificed and the primary tumor tissues were resected 10 h after treatment. The tissues were homogenized and the supernatant of tissue lysate was collected and stored at –20 °C. The quantities of IL-2 and IFN-γ in the plasma or tissue homogenate supernatant of the mice were determined by a Human Interleukin 2 ELISA Kit and a Human Interferon Gamma ELISA Kit (Cloud-Clone Corp., USA). The DOX concentrations in the plasma sample and the supernatant of the tumor homogenate were verified by HPLC, as described previously[57,58] with minor modifications. A 120 μL plasma sample was deproteinized with 380 μL of acetonitrile, and 120 μL of methanol containing 1 mg mL^{-1} of daunorubicin hydrochloride (internal standard) was added. After vigorous stirring and centrifugation (13 000 rpm, 10 min), 500 μL of supernatant was collected and evaporated under a stream of nitrogen at ambient temperature. The dried samples were dissolved in 100 μL of a mobile phase and then injected onto a reversed-phase (RP) HPLC column (C18). The mobile phases, acetonitrile: KH_2PO_4 (pH 4.0, 30 mM) (70:30, v/v) with 0.1% (v/v) triethylamine (TEA), were run at a flow rate of 1.2 mL min^{-1}. The Waters Alliance HPLC system consisted of a Waters 2690 separation module and a Waters 2475 multi λ fluorescence detector was used, with the excitation and emission wavelengths set at 480 nm and 590 nm, respectively.

Animal and Tumor Xenograft Models: The in vivo antitumor efficacy of drug-loaded nPCGs was evaluated using the five-week-old male BALB/c nude mice (SLRC Laboratory Animal Company, P. R. China) inoculated with A549 cells subcutaneously in the right anterior flank of the mice. Treatments were given when the tumors in the mice reached a tumor volume of around 70 mm^3. The mice were weighed and randomly divided into 6 groups (n = 5), and 120 μL of PBS, free DOX (1.1 mg kg^{-1}) plus free proteins (IL-2: 1.25×10^7 IU kg^{-1}; IFN-γ: 0.87×10^7 IU kg^{-1}), blank nPCGs, nPCGs with DOX (1.1 mg kg^{-1}), nPCGs with proteins (IL-2: 1.25×10^7 IU kg^{-1}; IFN-γ: 0.87×10^7 IU kg^{-1}), and nPCGs with DOX (1.1 mg kg^{-1}) plus proteins (IL-2: 1.25×10^7 IU kg^{-1}; IFN-γ: 0.87×10^7 IU kg^{-1}) were subcutaneously injected beside the tumor using a 1.0 mL syringe. The tumor sizes were measured with vernier callipers using two perpendicular diameters every 2 days and the tumor volume was expressed using $V = a \times b^2/2$, where a was the longer diameter and b was the shorter diameter. The average body weight in each group was assessed simultaneously as an indicator of systemic toxicity. The care and use of the laboratory animals was performed in compliance with the protocols approved by the Animal Experimental Center of the Bethune Medical School of Jilin University Institutional Animal Care and Use Committee.

Histology and Immunohistochemistry: The tumors and major organs (heart, liver, spleen, lung, and kidney) were fixed in 4% PBS buffered paraformaldehyde and embedded in paraffin wax. The paraffin-embedded 4-μm sections were stained with hematoxylin and eosin (H&E) to assess the histology. In situ terminal deoxynucleotidyl transferase–mediated deoxyuridine triphosphate–nick end labeling (TUNEL) assay was carried out using an in situ cell death detection kit, fluorescein (ROCHE Molecular Biochemicals) to detect the cells undergoing DNA fragmentation associated with apoptosis according to the manufacturer's instruction, and the nuclei of the tumor cells were stained green. The apoptosis of cells was observed and analyzed by LSM 780 confocal laser-scanning microscopy (Zeiss). Primary antibody rabbit monoclonal antiactive Caspase 3 (Abcam, UK) and secondary antibody horseradish peroxidase (HRP)-conjugated goat anti-rabbit immunoglobulin G (IgG) (Maixin Biotech. Co., Fujian, P. R. China) were used for Caspase 3 immunohistochemistry staining. Primary antibody rabbit polyclonal anti-Ki-67 (Chemicon Merck Millipore) and secondary antibody HRP-conjugated goat anti-rabbit IgG (Maixin Biotech. Co., Fujian, P. R. China) were used for Ki-67 immunohistochemistry staining. Nuclei were labeled using 4,6-diamidino-2-phenylindole (DAPI). The positive ratio (for TUNEL, Caspase 3, and Ki-67) was designated as the normalization of positive cell number in each treated group to that in the control group and quantitatively analyzed using ImageJ software (US National Institutes of Health).

Quantitative Real-time PCR: The expression of apoptosis-related genes in tumor tissues was analyzed by quantitative real-time PCR (qPCR). The

© 2015 WILEY-VCH Verlag GmbH & Co. KGaA, Weinheim

resulting cDNA (STAT5, STAT1, Caspase 9, Bax, Caspase 3, and Bcl-2) were amplified by qPCR using β-actin as an internal control gene. Total RNA was isolated from tumor tissues using Trizol reagent (Invitrogen) and the amount of pure RNA was quantified using a Tecan Infinite M200 plate reader with A260/280 greater than 1.90. Purified RNA was then reverse transcribed into cDNA by a reverse transcription kit (Takara, Japan). qPCR was performed using a SYBR Premix Ex Taq Real-time PCR kit (Takara, Japan) on a Stratagene MxPro3005 system. The genome structures of apoptosis-related genes Caspase 3, Caspase 9, Bcl-2, Bax, STAT5, STAT1, and the housekeeping gene, β-actin, were determined and the gene-specific primers for amplification were designed and are listed in Table S1 (Supporting Information). Calculation of the relative expression level of the apoptotic genes was performed using β-actin as the reference gene to obtain normalized gene expression values.

Statistical analysis: Data from all measurements of in vitro and in animal studies are shown as mean ± standard deviation (SD). Statistical comparisons were analyzed by the paired Student's *t* test or one-way ANOVA with a 95% confidence interval. $^{*}P < 0.05$ was considered statistically significant. $^{**}P < 0.01$ and $^{***}P < 0.001$ were considered extremely significant.

Supporting Information

Supporting Information is available from the Wiley Online Library or from the author.

Acknowledgements

We gratefully acknowledge support from the National Natural Science Foundation of China (projects 21174142, 51233004, 51390484 and 51321062) and the Ministry of Science and Technology of China (International cooperation and communication program 2011DFR51090).

Received: July 5, 2015
Revised: August 11, 2015
Published online: October 8, 2015

[1] T. Akao, T. Kimura, Y.-s. Hirofuji, K. Matsunaga, R. Imayoshi, J.-i. Nagao, T. Cho, H. Matsumoto, S. Ohtono, J. Ohno, *J. Drug Targeting* **2010**, *18*, 550.
[2] G. Cavaletti, P. Marmiroli, *Nat. Rev. Neurol.* **2010**, *6*, 657.
[3] A. Prahallad, C. Sun, S. Huang, F. Di Nicolantonio, R. Salazar, D. Zecchin, R. L. Beijersbergen, A. Bardelli, R. Bernards, *Nature* **2012**, *483*, 100.
[4] B. Deng, *Nat. Med.* **2015**, *21*, 105.
[5] S.-M. Lee, T. V. O'Halloran, S. T. Nguyen, *J. Am. Chem. Soc.* **2010**, *132*, 17130.
[6] M. Zheng, C. Yue, Y. Ma, P. Gong, P. Zhao, C. Zheng, Z. Sheng, P. Zhang, Z. Wang, L. Cai, *ACS Nano* **2013**, *7*, 2056.
[7] Z. Chen, K. Cheng, Z. Walton, Y. Wang, H. Ebi, T. Shimamura, Y. Liu, T. Tupper, J. Ouyang, J. Li, *Nature* **2012**, *483*, 613.
[8] A. Ribas, F. S. Hodi, M. Callahan, C. Konto, J. Wolchok, *New Engl. J. Med.* **2013**, *368*, 1365.
[9] P. Warde, M. Mason, K. Ding, P. Kirkbride, M. Brundage, R. Cowan, M. Gospodarowicz, K. Sanders, E. Kostashuk, G. Swanson, *The Lancet* **2012**, *378*, 2104.
[10] N. D. James, S. A. Hussain, E. Hall, P. Jenkins, J. Tremlett, C. Rawlings, M. Crundwell, B. Sizer, T. Sreenivasan, C. Hendron, *New Engl. J. Med.* **2012**, *366*, 1477.
[11] H. Meng, M. Liong, T. Xia, Z. Li, Z. Ji, J. I. Zink, A. E. Nel, *ACS Nano* **2010**, *4*, 4539.
[12] A. M. Scott, J. D. Wolchok, L. J. Old, *Nat. Rev. Cancer* **2012**, *12*, 278.
[13] S. Mocellin, C. R. Rossi, P. Pilati, D. Nitti, *Cytokine Growth Factor Rev.* **2005**, *16*, 35.
[14] G. Dranoff, *Nat. Rev. Cancer* **2004**, *4*, 11.
[15] G. K. Schwartz, D. Ward, L. Saltz, E. S. Casper, T. Spiess, E. Mullen, J. Woodworth, R. Venuti, P. Zervos, A. Storniolo, *Clin. Cancer. Res.* **1997**, *3*, 537.
[16] A. Ohtsu, M. A. Shah, E. Van Cutsem, S. Y. Rha, A. Sawaki, S. R. Park, H. Y. Lim, Y. Yamada, J. Wu, B. Langer, *J. Clin. Oncol.* **2011**, *29*, 3968.
[17] H. T. Ta, C. R. Dass, I. Larson, P. F. Choong, D. E. Dunstan, *Biomaterials* **2009**, *30*, 3605.
[18] A. Bodley, L. F. Liu, M. Israel, R. Seshadri, Y. Koseki, F. C. Giuliani, S. Kirschenbaum, R. Silber, M. Potmesil, *Cancer Res.* **1989**, *49*, 5969.
[19] S. Wang, E. A. Konorev, S. Kotamraju, J. Joseph, S. Kalivendi, B. Kalyanaraman, *J. Biol. Chem.* **2004**, *279*, 25535.
[20] S. Eikawa, M. Nishida, S. Mizukami, C. Yamazaki, E. Nakayama, H. Udono, *Proc. Natl. Acad. Sci. USA* **2015**, *112*, 1809.
[21] H. Tsukamoto, S. Senju, K. Matsumura, S. L. Swain, Y. Nishimura, *Nat. Commun.* **2015**, *6*, 6702.
[22] W. Liao, J.-X. Lin, W. J. Leonard, *Immunity* **2013**, *38*, 13.
[23] S. A. Rosenberg, J. R. Yannelli, J. C. Yang, S. L. Topalian, D. J. Schwartzentruber, J. S. Weber, D. R. Parkinson, C. A. Seipp, J. H. Einhorn, D. E. White, *J. Natl. Cancer Inst.* **1994**, *86*, 1159.
[24] S. E. Ealick, W. J. Cook, S. Vijay-Kumar, M. Carson, T. L. Nagabhushan, P. P. Trotta, C. E. Bugg, *Science* **1991**, *252*, 698.
[25] E. F. Wheelock, *Science* **1965**, *149*, 310.
[26] M. E. Gleave, M. Elhilali, Y. Fradet, I. Davis, P. Venner, F. Saad, L. H. Klotz, M. J. Moore, V. Paton, A. Bajamonde, *New Engl. J. Med.* **1998**, *338*, 1265.
[27] S. Marrache, S. Tundup, D. A. Harn, S. Dhar, *ACS Nano* **2013**, *7*, 7392.
[28] A. L. Lee, V. W. Ng, S. Gao, J. L. Hedrick, Y. Y. Yang, *Adv. Funct. Mater.* **2014**, *24*, 1538.
[29] M. C. Giano, Z. Ibrahim, S. H. Medina, K. A. Sarhane, J. M. Christensen, Y. Yamada, G. Brandacher, J. P. Schneider, *Nat. Commun.* **2014**, *5*, 4095.
[30] J.-A. Yang, J. Yeom, B. W. Hwang, A. S. Hoffman, S. K. Hahn, *Prog. Polym. Sci.* **2014**, *39*, 1973.
[31] F. P. Seib, E. M. Pritchard, D. L. Kaplan, *Adv. Funct. Mater.* **2013**, *23*, 58.
[32] K. M. Park, S. Gerecht, *Nat. Commun.* **2014**, *5*, 4075.
[33] J. Kopeček, J. Yang, *Angew. Chem. Int. Ed.* **2012**, *51*, 7396.
[34] B. V. Slaughter, S. S. Khurshid, O. Z. Fisher, A. Khademhosseini, N. A. Peppas, *Adv. Mater.* **2009**, *21*, 3307.
[35] Y. Li, J. Rodrigues, H. Tomas, *Chem. Soc. Rev.* **2012**, *41*, 2193.
[36] S. J. Buwalda, K. W. Boere, P. J. Dijkstra, J. Feijen, T. Vermonden, W. E. Hennink, *J. Controlled Release* **2014**, *190*, 254.
[37] D. Seliktar, *Science* **2012**, *336*, 1124.
[38] D. Ding, Z. Zhu, R. Li, X. Li, W. Wu, X. Jiang, B. Liu, *ACS Nano* **2011**, *5*, 2520.
[39] M. Molinos, V. Carvalho, D. M. Silva, F. M. Gama, *Biomacromolecules* **2012**, *13*, 517.
[40] M. Huang, H. Furukawa, Y. Tanaka, T. Nakajima, Y. Osada, J. P. Gong, *Macromolecules* **2007**, *40*, 6658.
[41] R. N. Winter, A. Kramer, A. Borkowski, N. Kyprianou, *Cancer Res.* **2001**, *61*, 1227.
[42] J. Bullwinkel, B. Baron-Lühr, A. Lüdemann, C. Wohlenberg, J. Gerdes, T. Scholzen, *J. Cell. Physiol.* **2006**, *206*, 624.
[43] J. Savill, *Kidney Int.* **1999**, *56*, 1216.
[44] J. E. Darnell, *Science* **1997**, *277*, 1630.
[45] L. Rocha-Zavaleta, C. Huitron, J. R. Cacéres-Cortés, J. A. Alvarado-Moreno, A. Valle-Mendiola, I. Soto-Cruz, B. Weiss-Steider, R. Rangel-Corona, *Cell. Signal.* **2004**, *16*, 1239.

© 2015 WILEY-VCH Verlag GmbH & Co. KGaA, Weinheim

[46] M.-H. Zhu, S. John, M. Berg, W. J. Leonard, *Cell* **1999**, *96*, 121.
[47] M. T. Nevalainen, J. Xie, J. Torhorst, L. Bubendorf, P. Haas, J. Kononen, G. Sauter, H. Rui, *J. Clin. Oncol.* **2004**, *22*, 2053.
[48] J. Darnell, I. M. Kerr, G. R. Stark, *Science* **1994**, *264*, 1415.
[49] S. Walker, E. Nelson, D. Frank, *Oncogene* **2007**, *26*, 224.
[50] L. T. Vassilev, B. T. Vu, B. Graves, D. Carvajal, F. Podlaski, Z. Filipovic, N. Kong, U. Kammlott, C. Lukacs, C. Klein, *Science* **2004**, *303*, 844.
[51] H. Zheng, H. You, X. Z. Zhou, S. A. Murray, T. Uchida, G. Wulf, L. Gu, X. Tang, K. P. Lu, Z.-X. J. Xiao, *Nature* **2002**, *419*, 849.
[52] T. Rossé, R. Olivier, L. Monney, M. Rager, S. Conus, I. Fellay, B. Jansen, C. Borner, *Nature* **1998**, *391*, 496.
[53] M. S. Soengas, R. Alarcon, H. Yoshida, R. Hakem, T. Mak, S. Lowe, *Science* **1999**, *284*, 156.
[54] R. D. Schreiber, L. J. Old, M. J. Smyth, *Science* **2011**, *331*, 1565.
[55] U. Hammerling, A.-C. Henningsson, L. Sjödin, *J. Pharm. Biomed. Anal.* **1992**, *10*, 547.
[56] F. Gu, R. Neufeld, B. Amsden, *J. Controlled Release* **2007**, *117*, 80.
[57] H.-J. Cho, I.-S. Yoon, H. Y. Yoon, H. Koo, Y.-J. Jin, S.-H. Ko, J.-S. Shim, K. Kim, I. C. Kwon, D.-D. Kim, *Biomaterials* **2012**, *33*, 1190.
[58] R. F. Greene, J. M. Collins, J. F. Jenkins, J. L. Speyer, C. E. Myers, *Cancer Res.* **1983**, *43*, 3417.

© 2015 WILEY-VCH Verlag GmbH & Co. KGaA, Weinheim